ADVANCED MATERIALS TECHNOLOGIES
www.advmattechnol.de

3D-Printed Photonic Crystal Sub-Terahertz Leaky-Wave Antenna

Hichem Guerboukha, Masoud Sakaki, Rabi Shrestha, Jingwen Li, Johanna Kölbel, Niels Benson, and Daniel M. Mittleman*

Wireless systems are facing increasing pressure due to the growing demand for data transmission. One potential solution to this problem is to shift communication frequencies toward the terahertz (THz) spectrum. However, this requires the development of new components that can efficiently process signals at these high frequencies and transmit them via highly directional beams. In this study, a novel approach is proposed to achieving efficient THz signal processing by combining two existing technologies: photonic crystals and leaky-wave antennas. Incorporating a 2D photonic crystal inside a leaky-wave waveguide allows to manipulate the wave vector of the guided wave in unique ways, which in turn impacts the far-field radiation pattern emitted through the leaky-wave aperture. The device fabrication uses 3D printing of alumina and allows for convenient and scalable manufacturing. Through numerical simulations and experiments, free-space data transmission at rates of few hundred Mbps at a carrier frequency of 101.2 GHz is demonstrated. The findings illustrate the feasibility of photonic crystal-based leaky-wave antennas and lay the groundwork for the development of compact and high-performance components for THz wireless communication systems.

1. Introduction

Wireless communication systems are currently facing significant challenges in meeting the growing demand for high-speed data transmission.[1] Recent research has focused on the potential of utilizing carrier frequencies in the millimeter-wave and THz bands (>100 GHz) for this purpose,[2] as these frequencies offer wide bandwidths that can support ultrahigh-speed data transmission.[3–5] However, working at such high frequencies also presents a number of challenges, including free-space path loss (FSPL), which can be as high as ≈80 dB at 300 GHz for a 1 m distance. One strategy for addressing these challenges is the use of highly directional antennas, such as leaky-wave antennas that can be designed to achieve high antenna gains.

Leaky-wave antennas have been extensively studied in the microwave range for several years,[6–9] but have only recently been proposed as a solution for THz communications.[10] The simplest leaky-wave antenna is created by cutting a slot along the length of a waveguide, which allows the wave to emerge from the waveguide at a frequency-dependent angle. The produced "rainbow" pattern has been demonstrated in a variety of THz applications, including beam steering,[11,12] frequency-division multiplexing,[13,14] link discovery,[15] radar,[16,17] and THz identification tags.[18] The functionality of a leaky-wave antenna is determined by the characteristics of the propagating mode, specifically its wavevector β. Indeed, for a leaky-wave antenna with a single slot, the energy leaks at the angle $\cos\theta = \beta/k_0$, where $k_0 = \omega/c$ is the free-space wavevector. Therefore, by manipulating the guided wave's wavevector, it is possible to control the far-field radiation pattern of the antenna.

In that regard, the photonic crystal platform is a remarkable tool for efficient manipulation of wave propagation in confined guided structures.[19,20] Photonic crystals are artificial, periodic structures that control the propagation of light, similar to how electrons are affected by ionic lattices. By judiciously designing the geometry and material properties of their constituents, photonic bandgaps can be induced in the band diagram. By introducing a defect in the geometry, the direction of light propagation can be controlled. Photonic crystals have been extensively studied as photonic components for guiding and manipulating optical signals in the optical region over the past few decades.

H. Guerboukha
School of Science and Engineering
University of Missouri-Kansas City
Kansas City, MO 64110, USA
E-mail: hichem.guerboukha@umkc.edu
M. Sakaki, N. Benson
Institute of Technology for Nanostructures and Technology
Univesität Duisburg-Essen
47057 Duisburg, Germany
R. Shrestha, J. Kölbel, D. M. Mittleman
School of Engineering
Brown University
Providence, RI 02912, USA
J. Li
School of Science
Jiangnan University
1800 Lihu Ave, Wuxi 214122, China

The ORCID identification number(s) for the author(s) of this article can be found under https://doi.org/10.1002/admt.202300698

DOI: 10.1002/admt.202300698

In the THz range, several types of THz photonic crystal waveguides have been proposed.[21] These include Bragg waveguides [22–24] and hyperuniform disordered waveguides [25] for wave propagation,[26–28] sensing,[29,30] and communications.[31,32] Most of these waveguides were designed to confine radiation throughout their length, making them unidimensional photonic crystal fibers. To develop compact components for diverse THz manipulations, such as multiplexing and routing of terahertz waves, photonic crystal waveguides can also be implemented in 2D photonic slabs. For example, Withayachumnankul et al. reported a photonic slab with a hexagonal array of air holes for efficient guiding and manipulation of THz waves.[33] By introducing a line defect in the periodicity, a waveguiding structure is created. The clad region around the defect provides the bandgap effect and results in wave confinement in the in-plane dimensions, while total internal reflection prevents radiation leakage into free space in the vertical direction. With this configuration, a frequency-division triplexer has been experimentally realized on the photonic crystal platform.[34]

Although various configurations of 2D photonic crystal slabs have been reported in the THz region ,[34–38] there have been relatively few studies that focus on the detailed design of antennas based on photonic crystals.[39] Antennas are crucial for coupling guided waves into free space, which is a key challenge for realizing THz wireless communications. In this work, we propose an alternative photonic crystal design that enables free-space coupling using a leaky-wave mechanism. Previous reported photonic crystals have primarily used a hole-in-dielectric design, which supports a slow wave mode with a phase constant $\beta > k_0$. These modes require the introduction of periodic scatterers (e.g., periodic slots) to excite free-space Floquet modes.[8,40] In contrast, we use a cylinder-in-air design that produces fast-wave modes ($\beta < k_0$) where the in-plane confinement is ensured by sandwiching the structure between two metallic plates.[41] While similar designs of high-permittivity cylinders have been proposed at optical wavelengths,[42–44] their fabrication is more complicated and involves a series of complex microfabrication steps, such as electron-beam lithography, to carve the cylinders. At THz frequencies, our approach is possible due to the recent advancements in 3D printing technology of alumina, a high permittivity ceramic material. By removing a row of cylinders, we effectively introduce a linear defect that allows a fast-wave mode with a phase constant $\beta < k_0$. By cutting a thin slot on the metallic plate directly above the linear defect, we can efficiently leak energy out of the waveguide. We then demonstrate its practical applicability by implementing it in a communication system.

2. Design and Fabrication of the Photonic Crystal

Figure 1a illustrates a schematic of the photonic crystal alongside microscopy image of the fabricated sample. The crystal is composed of an array of alumina (Al_2O_3) cylinders arranged in a square lattice with a lattice constant of 1.06 mm. Alumina is selected for its large refractive index ($n = 3.08$) and low absorption losses ($\alpha = 0.0024$ cm^{-1}) around 100 GHz.[45] These values can be compared to typical materials used to fabricate PCB. For example, the Rogers RT/duroid 6010.2LM has a similar refractive index ($n = 3.19$) but significantly larger losses ($\alpha = 1.36$ cm^{-1}).[46]

A square array of cylinders of high permittivity material can open a bandgap for the out-of-plane polarization (TM mode).[41] The 390 µm diameter cylinders are placed on a flat, 160 µm thick rectangular plate, which is also alumina, and serves as a mechanical support. The fabricated device has dimensions of 30 mm x 43 mm, a thickness of 0.860 mm, and is sandwiched between two 1-mm thick aluminum plates to allow propagation as in a parallel plate waveguide.[47] Here, the plate separation is chosen such that only the fundamental TM mode is excited. We note that the cutoff for the TM_1 mode is $f_1 = 1/(2d\sqrt{\mu_0\epsilon_0\epsilon_r})$, where d is the plate separation, ϵ_0 and μ_0 the vacuum permittivity and permeability respectively, and ϵ_r the effective permittivity. For a waveguide where the medium between the plates was made entirely of alumina, the plate separation must be smaller than ≈0.4 mm to avoid excitation of the second order mode (and therefore multimode propagation). In our case, since the waveguide is made of an array of alumina cylinders in air, the effective permittivity depends on the volume contribution of the air-to-alumina ratio, which brings the effective permittivity closer to 1, and thus requires a larger plate separation. In practice, we simulated various plate separations to find the best geometry that allows single-mode operation.

Figure 1b presents the calculated band diagram of the resulting photonic crystal. This was obtained using a commercial finite element method solver. Because of the repeated geometry, we simulate only one unit cell, i.e., only one cylinder with its bottom alumina plate (as shown in Figure 1a). We use perfect electric conductor boundaries for the top and bottom, and Floquet periodicity boundary conditions on the sides to simulate the infinitely periodic medium. We perform a parametric sweep over the wavevector and the finite element software solves for the corresponding eigenproblem. Specifically, for a given wavevector, it finds eigenfrequencies (eigenvalues) and electric field mode distribution (eigenvectors). The former are used to obtain the band diagram, while the latter can be used to show corresponding electric fields.

As can be seen, the geometry opens a bandgap around 105 GHz with a bandwidth of ≈11 GHz, resulting in a relative bandgap of $\Delta f/f_0 = 11\%$, which can be compared to alternative photonic crystal designs at higher THz frequencies: using silicon photonic crystal slab ($\Delta f/f_0 = 2.8\%$ with $f_0 = 326.5$ GHz [36]), metallic photonic crystal ($\Delta f/f_0 = 59\%$ with $f_0 = 850$ GHz[35]), and hybrid metal-dielectric photonic crystal ($\Delta f/f_0 = 19\%$ with $f_0 = 380$ GHz[28]). We note that to shift the bandgap towards higher frequencies, one would need to scale down the size of the structure. In theory, the minimum size for the cylinders is 25 µm, i.e., the pixel size of the 3D printer. However, due to practical limitations, such as difficulty in post-processing cleaning, cylinders smaller than 100 µm are not printable. Our simulations show that, for example, assuming 100 µm cylinders and a base thickness of 50 µm would yield bandgap in the 310–345 GHz range.

The photonic crystal was fabricated using a LITHOZ CeraFab7500 3D printer, which has a lateral resolution of 25 µm and employs LCM (Lithography-based Ceramic Manufacturing) technology. LCM utilizes a DLP projector combined with a UV light for selective, layer-by-layer polymerization of a photo-sensitive slurry. In this research, the employed slurry (LithaLox 360) consisted of 49 Vol% Al_2O_3 powder mixed with 51 Vol% polymer, and the printing layer height and energy were 25 µm and 430 mJ cm^{-2}, respectively.

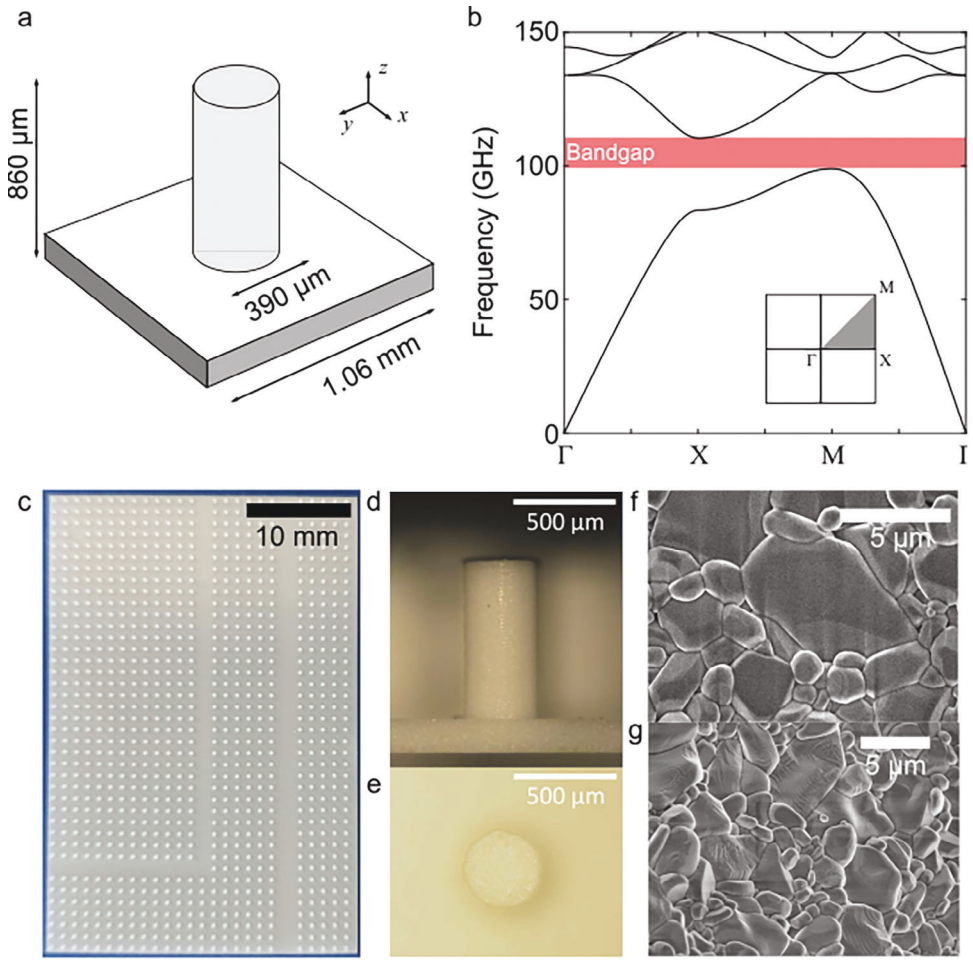

Figure 1. a) Geometry of the unit cell of the photonic crystal. The cylinders rest on a planar plate for structural rigidity. b) Resulting band diagram. c) Photograph (top view) of the fabricated sample. d) Microscope images of the side view and e) top view. f) Scanning electron microscope image of the sample's surface and g) cross-section.

Immediately following printing, the excess slurry was removed from the surface of the sample using LithaSol 20 cleaning fluid. The sample then underwent several thermal-processing steps in an ambient atmosphere to convert the printed part into a dense and firm sample. These steps can be grouped into three categories: drying, debinding (i.e., removing the polymer from the sample) and sintering. The key here is that the heating rate should be low enough to guarantee the safe removal of the polymer (and other volatile compounds) from the sample. In this study, the maximum sintering temperature was 1600 °C and the dwell time at this temperature was 2 h. Further details about the alumina processing can be found in Ref.[48].

A photograph of the fabricated sample is shown in Figure 1c, while microscope images are presented in Figure 1d (side view) and Figure 1e (top view). Imperfections in the resulting sample, such as the layered structure of the cylinders, are deeply subwavelength, therefore the wave at 100 GHz (wavelength of 3 mm) is not affected by them. Scanning electron microscope (SEM: JEOL JSM 7500) image shown in Figure 1f reveals grain size at the surface of the alumina sample in the order of a few micrometers, which again is much less than the wavelength. We also performed a cross-section of the sample (Figure 1g) and observe a similar grain size within the volume of the object. These measurements suggest that the effective medium theory can apply such that the wave observes a uniform permittivity within the volume of the material.

One of the key advantages of the photonic crystal platform is its ability to route radiation along a given direction when a defect is introduced in the crystal structure. For example, in our sample, a linear defect is introduced by removing a row of cylinders, while keeping the bottom alumina plate for structural integrity. **Figure 2a** shows the calculated resulting relation dispersion for k_x, i.e., in the $\Gamma \rightarrow X$ direction. As shown, a unique defect mode exists in the bandgap (green curve in Figure 2a). The electric field distribution shown in Figure 2b and Figure 2c reveals that the mode is polarized parallel to the cylinders (out-of-plane, in the z direction), and is mainly localized in the defect (the missing row). Our numerical simulations show that the losses of the defect mode (assuming an aluminum conductivity of 3.774×10^7 S m^{-1}) are 7 dB cm^{-1}. These losses can be divided in two parts: material losses and ohmic losses. Material losses are very small,

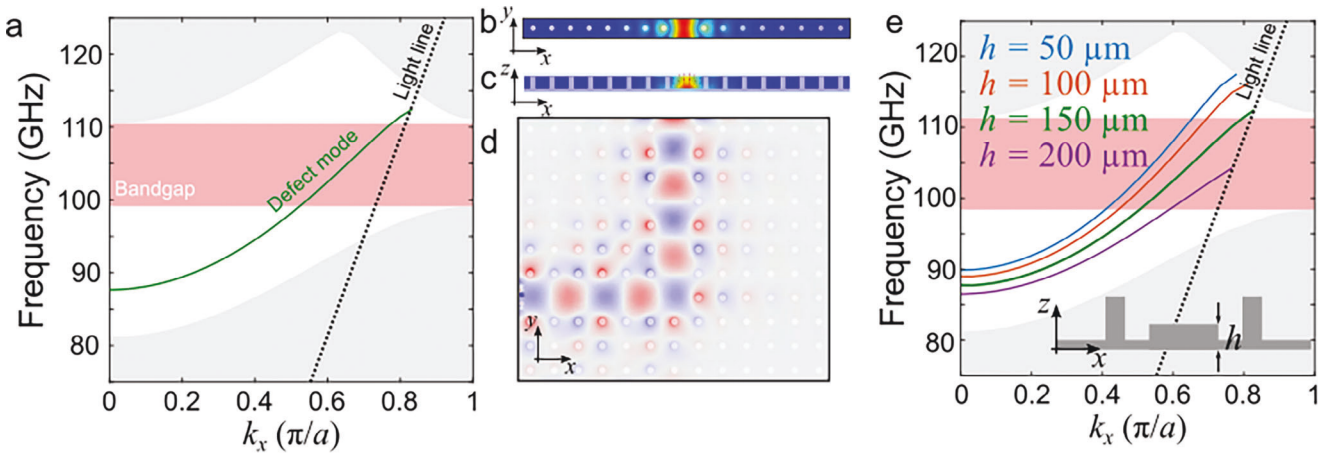

Figure 2. a) The band diagram in the $\Gamma \rightarrow X$ direction for the photonic crystal with a linear defect. Here, the defect consists of removing one row of cylinders while keeping the base 155 μm alumina for structural support. The green curve shows the unique defect mode that exists in the bandgap. b) Top view and c) side view of the electric field distribution of the defect mode polarized in the *z* direction. The mode is localized in the defect. d) Propagation of the wave along a L-shaped defect. e) The defect mode can be engineered, for example by geometrically changing the thickness h of the base plate.

since the field is either located in air (virtually lossless) or in the alumina (0.011 dB cm^{-1}). In contrast, ohmic losses are significant. Indeed, we note that the defect mode is polarized similarly to that of a TEM mode in a dielectric-filled parallel plate waveguide. In such a mode, when the dielectric is alumina, losses can be analytically calculated to be 8.36 dB cm^{-1}.[49] This confirms that ohmic losses are the main contributor to the losses we found numerically.

When THz waves of vertical polarization are injected at the input port, they can excite this mode and propagate along the defect if their frequency is in the bandgap. This is demonstrated in Figure 2d for an L-shaped defect. Furthermore, it is worth noting that the dispersion relation can be tailored by geometrical optimization of the defect structure. For example, Figure 2e shows how the wavevector of the defect mode changes when the plate thickness is varied in the region where the missing cylinder used to be, from 50 to 200 μm.

Our fabricated sample features two channels, namely an L-shaped defect and straight linear defect (Figure 1c). First, we demonstrate propagation through the L-shaped defect. We employ a THz time-domain spectroscopy system to inject vertically polarized THz waves at the input of the L-shaped defect and we measure the radiation emerging from the photonic crystal at the opposite end of the L-shaped defect (inset to **Figure 3a**). In our experiment, the wave is radiated in free space, before being focused at the input end of the defect channel with a combination of biconvex lens and tapered waveguide input.[50] The measured spectrum shown in Figure 3a reveals a peak around 105 GHz,

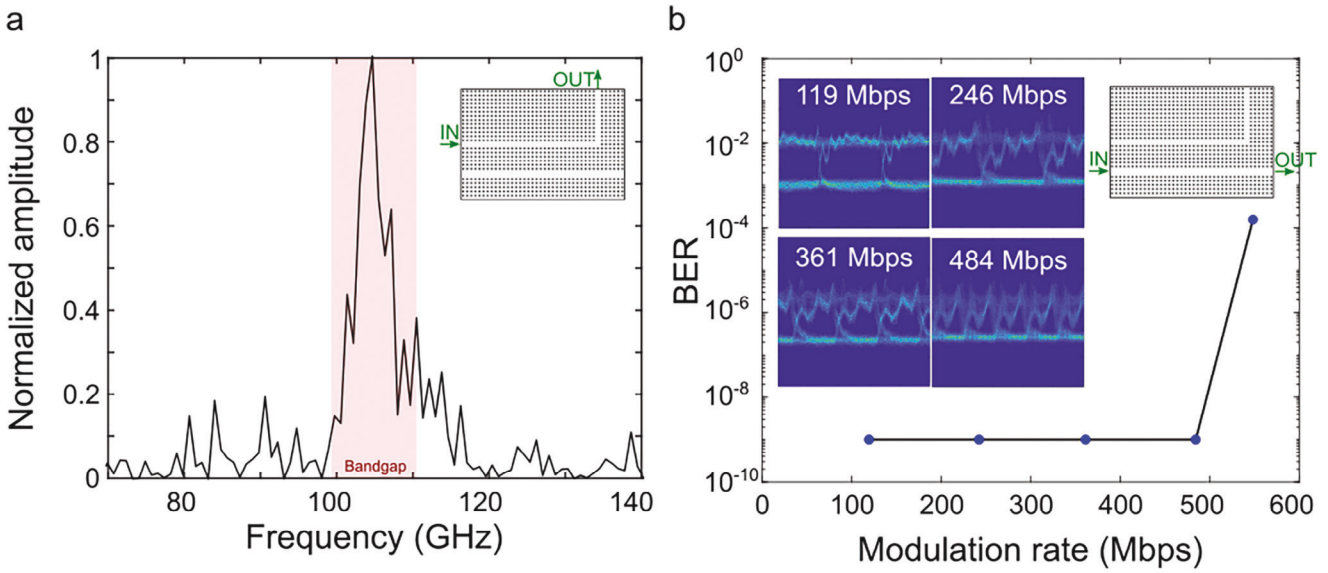

Figure 3. a) Measured spectrum from a THz time-domain measurement when light in injected at one end of the L-shaped defect and measured at the other end (as shown in inset). b) Bit error rate for different modulation rate for a center frequency of 101.2 GHz, measured through the straight channel (as shown in inset). Inset shows measured eye diagrams for various modulation rates.

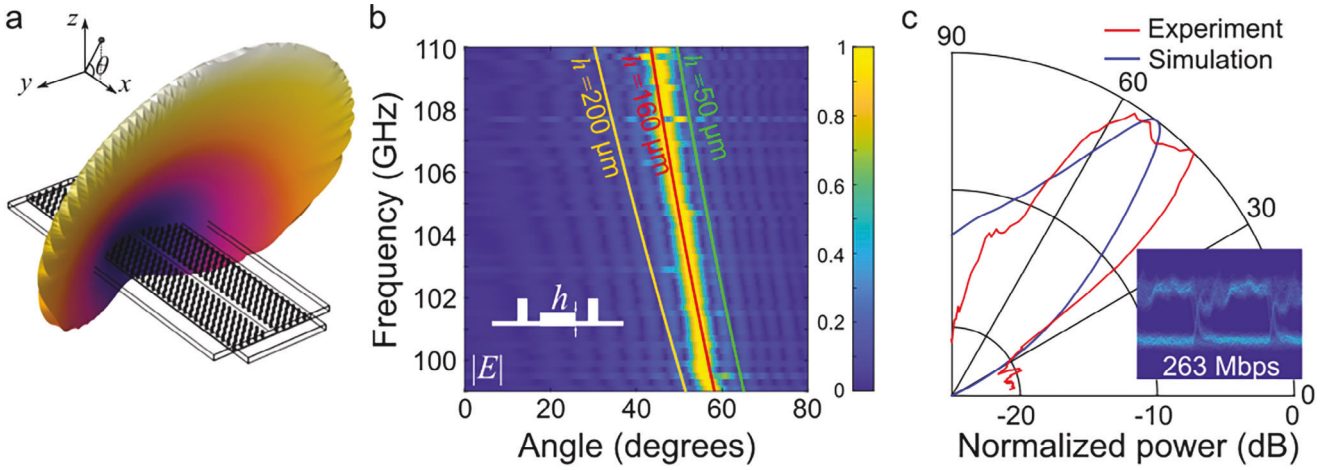

Figure 4. a) 3D radiation pattern of the photonic crystal leaky-wave antenna for the bandgap frequency of 105 GHz. b) Simulated radiation pattern for the frequencies in the bandgap in the *xz*-plane. The red curve is the angle deduced from the dispersion relation of the defect mode. c) Measured power (in the *xz*-plane) as a function of the angle (red) compared to the simulation (blue) for a modulated signal centered at a frequency of 101.2 GHz. Inset shows the eye diagram at an angle of 50°.

confirming that the photonic crystal functions as intended, and that only frequencies in the bandgap can propagate along the L-shaped channel.

Next, we confirm that the defect channel can support real-time transmission of data through the straight channel. For that purpose, we modulate a 12.65 GHz RF signal using a double balanced mixer driven by a pulse pattern generator outputting an on-off keying (OOK) signal with a pseudo-random binary sequence of length $2^7 - 1$. The modulated signal is routed through a frequency multiplier chain with a multiplication factor of 8, allowing the generation a modulated signal centered at 101.2 GHz.[51] To couple the wave into the waveguide, we use a similar strategy as with the TDS measurements using a tapered waveguide input. After propagating through the channel, the signal is collected by a waveguide-coupled zero-bias Schottky diode. The signal passes through low-pass filters to obtain the baseband signal between 0.1 MHz and 6 GHz, before being routed to a power meter, an oscilloscope to provide eye diagrams, or a real-time bit error rate (BER) tester. Figure 3b shows the measured BER as a function of the modulation rate, confirming that the photonic crystal can support transmission data up to 500 Mbps. As can be seen in the eye diagrams (inset of Figure 3b), the signal gets more distorted as the modulation rate increases. This is related to the fact that, as the bandwidth increases, the lower edge of the spectrum goes outside of the photonic bandgap, for the particular center frequency of our communication system (see bandgap in Figure 3a). We note that, in principle, one could increase the potential data rates by operating at a carrier frequency in the center of the bandgap. Also, we mention that a photonic crystal similar to the one presented here could be designed for frequency-division multiplexing.[52] This can take the form of introducing optical cavities in the form of point defects.[53] Ultimately, one could then use a photonic-crystal-based leaky-wave antenna to engineer the free-space frequency-dependent radiation pattern, i.e., leveraging frequency-division multiplexing to broadcast different frequency bands at different locations.[13]

3. Photonic Crystal Leaky-Wave Antenna

We now turn to the specific design of a leaky-wave antenna from the photonic crystal introduced earlier. From the dispersion relation of Figure 2a, we note that the defect mode is a fast-wave mode, meaning its wavevector is located in the radiation region above the air line $\beta < k_0$. By phase matching, this mode can therefore directly outcouple in free space at an elevation angle $\cos\theta = \beta/k_0$. This means that the output angle θ is a function of frequency. This outcoupling can be realized by simply introducing a thin linear slot in the metal plate located right above the defect.

Figure 4a shows the 3D radiated power at a frequency of 105 GHz for a slot width of 0.5 mm ($\lambda/6$). The radiated power peaks at an angle of ≈49° from the antenna. Figure 4b shows simulated radiation patterns for the frequencies located in the bandgap. As expected, the simulated peak pattern agrees well with the angle that can be derived from the phase matching condition, i.e., the frequency-dependent angles given by $\cos\theta = \beta/k_0$. This is shown as the red curve in Figure 4b. With our device, we can achieve an angular range of ≈16° for frequencies located in the bandgap. The peak angle can also be varied by adjusting the geometry of the defect, for example, the plate thickness h within the defect. Figure 4b illustrates this as the green and orange curves which depicts the predicted angle-frequency relationship when h is changed to 50 and 200 μm, respectively. This shows that engineering the dispersion constant is possible with a photonic crystal-based leaky-wave antenna. It is also worth mentioning the effect of the aperture geometry on the resulting radiated pattern.[10] In general, having a large slot width result in a lower antenna gain and narrower radiated peak, since most of the energy quickly leaks at the beginning of the slot (large leakage constant). Conversely, a long and thin slot may increase the directivity since the leaking energy is distributed on a geometrically longer effective aperture (small leakage constant).

Finally, to verify the capabilities of our device as a leaky-wave antenna, we perform experiments to characterize the far-field ra-

diation emitted from a slot aperture located directly above the photonic crystal defect. We cut a 1 mm wide slot in the top metallic plate to allow the wave to leak into free space. As above, we excite the guided mode by injecting vertically polarized THz waves at a center of frequency of 101.2 GHz modulated at a rate of 263 Mbps. Figure 4c shows the measured radiated power as a function of angle (red line). The results agree overall with the simulation (shown as a blue line). A clear open eye diagram with error-free transmission (BER < 10^{-9}) is measured at 50° (shown in inset) at a broadcast range of 65 cm which is in the far field regime of this emitting aperture.

4. Conclusion

In conclusion, we have presented a novel design for a leaky-wave antenna based on photonic crystals. This design allows more versatility in engineering β which is a significant advantage over standard leaky-wave antennas. By using an array of alumina cylinders on a square lattice and introducing a linear defect in the structure, we create a fast-wave mode that can efficiently outcouple in free space. We demonstrate this by measuring the radiated power at different angles and observing a peak at the angle predicted by the phase matching condition. Our device is able to achieve an angular range of ≈16° for frequencies located in the bandgap, and can transmit data in free space at a rate of 263 Mbps, limited by the overlap between the photonic band gap and the spectrum of the modulated signal. We also showed how the defect can be engineered to alter the radiation pattern, and change its peaking angle. The device fabrication, using 3D printing of the alumina, allows for convenient and scalable fabrication. Our results demonstrate the potential of photonic crystals in enabling spectrally efficient communication in the THz range and pave the way for the development of compact and efficient THz wireless communication systems.

Acknowledgements

This work was supported by the US National Science Foundation (NSF-1954780 and NSF-2211616), the Air Force Office of Scientific Research (FA9550-221-0412), the German Research Foundation (DFG) within the project CRC/TRR 196 MARIE, project C09, as well as by the "Ministerium für Kultur und Wissenschaft des Landes Nordrhein-Westfalen" within the terahertz.NRW project. H. Guerboukha kindly acknowledges support from Fonds de Recherche Québec - Nature et Technologies.

Conflict of Interest

The authors declare no conflict of interest.

Data Availability Statement

The data that support the findings of this study are available from the corresponding author upon reasonable request.

Keywords

3D printing, antenna, leaky wave, photonic crystal, terahertz communications

Received: November 7, 2023
Published online: January 25, 2024

[1] Cisco, Cisco Annual Internet Report (2018–2023) White Paper https://www.cisco.com/c/en/us/solutions/collateral/executive-perspectives/annual-internet-report/white-paper-c11-741490.html (accessed: March **2020**).
[2] T. Nagatsuma, G. Ducournau, C. C. Renaud, *Nat. Photonics* **2016**, *10*, 371.
[3] S. Koenig, D. Lopez-Diaz, J. Antes, F. Boes, R. Henneberger, A. Leuther, A. Tessmann, R. Schmogrow, D. Hillerkuss, R. Palmer, T. Zwick, C. Koos, W. Freude, O. Ambacher, J. Leuthold, I. Kallfass, *Nat. Photonics* **2013**, *7*, 977.
[4] T. Harter, C. Füllner, J. N. Kemal, S. Ummethala, J. L. Steinmann, M. Brosi, J. L. Hesler, E. Bründermann, A.-S. Müller, W. Freude, S. Randel, C. Koos, *Nat. Photonics* **2020**, *14*, 601.
[5] K. Nallappan, H. Guerboukha, C. Nerguizian, M. Skorobogatiy, *IEEE Access* **2018**, *6*, 58030.
[6] L. Goldstone, A. Oliner, *IRE Trans. Antennas Propag.* **1959**, *7*, 307.
[7] A. Oliner, D. R. Jackson, in *Antenna Engineering Handbook*, (Ed.: J. L. Volakis), McGraw Hill, New York **2007**, p. 12.
[8] D. R. Jackson, C. Caloz, T. Itoh, *Proc. IEEE* **2012**, *100*, 2194.
[9] L. Liu, C. Caloz, T. Itoh, *Electron. Lett.* **2002**, *38*, 1414.
[10] H. Guerboukha, R. Shrestha, J. Neronha, O. Ryan, M. Hornbuckle, Z. Fang, D. M. Mittleman, *Appl. Phys. Lett.* **2020**, *117*, 261103.
[11] M. Esquius-Morote, J. S. Gomez-Diaz, J. Perruisseau-Carrier, *IEEE Trans. Terahertz Sci. Technol.* **2014**, *4*, 116.
[12] X.-C. Wang, W.-S. Zhao, J. Hu, W.-Y. Yin, *IEEE Trans. Nanotechnol.* **2015**, *14*, 62.
[13] N. J. Karl, R. W. Mckinney, Y. Monnai, R. Mendis, D. M. Mittleman, *Nat. Photonics* **2015**, *9*, 717.
[14] J. Ma, N. J. Karl, S. Bretin, G. Ducournau, D. M. Mittleman, *Nat. Commun.* **2017**, *8*, 729.
[15] Y. Ghasempour, R. Shrestha, A. Charous, E. Knightly, D. M. Mittleman, *Nat. Commun.* **2020**, *11*, 2017.
[16] K. Murano, I. Watanabe, A. Kasamatsu, S. Suzuki, M. Asada, W. Withayachumnankul, T. Tanaka, Y. Monnai, *IEEE Trans. Terahertz Sci. Technol.* **2017**, *7*, 60.
[17] Y. Amarasinghe, R. Mendis, D. M. Mittleman, *Opt. Express* **2020**, *28*, 17997.
[18] Y. Amarasinghe, H. Guerboukha, Y. Shiri, D. M. Mittleman, *Opt. Express* **2021**, *29*, 20240.
[19] S. Noda, A. Chutinan, M. Imada, *Nature* **2000**, *407*, 608.
[20] M. Thorhauge, L. H. Frandsen, P. I. Borel, *Opt. Lett.* **2003**, *28*, 1525.
[21] K. Nallappan, H. Guerboukha, Y. Cao, G. Xu, C. Nerguizian, D. M. Mittleman, M. Skorobogatiy, in *Next Generation Wireless Terahertz Communication Networks*, (Eds: A. D. S. Ghafoor, M. H. Rehmani), CRC Press, Boca Raton FL **2021**, pp. 379–410.
[22] J. Li, K. Nallappan, H. Guerboukha, M. Skorobogatiy, *Opt. Express* **2017**, *25*, 4126.
[23] T. Ma, K. Nallapan, H. Guerboukha, M. Skorobogatiy, *Opt. Express* **2017**, *25*, 11009.
[24] Y. Cao, K. Nallappan, H. Guerboukha, T. Gervais, M. Skorobogatiy, *Opt. Express* **2019**, *27*, 27663.
[25] T. Ma, H. Guerboukha, M. Girard, A. D. Squires, R. Lewis, M. Skorobogatiy, *Adv. Opt. Mater.* **2016**, *4*, 2085.
[26] A. Markov, H. Guerboukha, M. Skorobogatiy, *J. Opt. Soc. Am. B* **2014**, *31*, 2587.
[27] S. Atakaramians, S. Afshar, V. T. M. Monro, D. Abbott, *Adv. Opt. Photonics* **2013**, *5*, 169.
[28] H. Li, M. X. Low, R. T. Ako, M. Bhaskaran, S. Sriram, W. Withayachumnankul, B. T. Kuhlmey, S. Atakaramians, *Adv. Mater. Technol.* **2020**, *5*, 2000117.
[29] J. Li, H. Qu, J. Wang, *Biomed. Opt. Express* **2020**, *11*, 2476.
[30] H. Guerboukha, G. Yan, O. Skorobogata, M. Skorobogatiy, *Adv. Opt. Mater.* **2014**, *2*, 1181.

[31] K. Nallappan, Y. Cao, G. Xu, H. Guerboukha, C. Nerguizian, M. Skorobogatiy, *Photonics Res.* **2020**, *8*, 1757.
[32] Y. Cao, K. Nallappan, H. Guerboukha, G. Xu, M. Skorobogatiy, *Optica* **2020**, *7*, 1112.
[33] W. Withayachumnankul, M. Fujita, T. Nagatsuma, *Adv. Opt. Mater.* **2018**, *6*, 1800401.
[34] M. Yata, M. Fujita, T. Nagatsuma, *Opt. Express* **2016**, *24*, 7835.
[35] A. L. Bingham, D. R. Grischkowsky, *IEEE Microwave Wireless Compon. Lett.* **2008**, *18*, 428.
[36] K. Tsuruda, M. Fujita, T. Nagatsuma, *Opt. Express* **2015**, *23*, 31977.
[37] R. Kakimi, M. Fujita, M. Nagai, M. Ashida, T. Nagatsuma, *Nat. Photonics* **2014**, *8*, 657.
[38] P. Gopalan, B. Sensale-Rodriguez, *Adv. Opt. Mater.* **2020**, *8*, 1900550.
[39] D. Headland, A. K. Klein, M. Fujita, T. Nagatsuma, *APL Photonics* **2021**, *6*, 096104.
[40] F. Xu, K. Wu, *IEEE Microwave Mag.* **2013**, *14*, 87.
[41] J. D. Joannopoulos, S. G. Johnson, J. N. Winn, R. D. Meade, *Photonic Crystals: Molding the Flow of Light*, Princeton University, Princeton NJ **2011**.
[42] P. R. Villeneuve, M. Piché, *Phys. Rev. B* **1992**, *46*, 4973.
[43] C.-C. Chen, C.-Y. Chen, W.-K. Wang, F.-H. Huang, C.-K. Lin, W.-Y. Chiu, Y.-J. Chan, *Opt. Express* **2005**, *13*, 38.
[44] W.-Y. Chiu, T.-W. Huang, Y.-H. Wu, Y.-J. Chan, C.-H. Hou, H. T. Chien, C.-C. Chen, *Opt. Express* **2007**, *15*, 15500.
[45] J. Ornik, M. Sakaki, M. Koch, J. C. Balzer, N. Benson, *IEEE Access* **2021**, *9*, 5986.
[46] Rogers, RT/duroid® 6006 and 6010.2LM Laminates, https://www.rogerscorp.com/advanced-electronics-solutions/rt-duroid-laminates/rt-duroid-6006-and-6010-2lm-laminates, (accessed: January 2024).
[47] R. Mendis, D. M. Mittleman, *J. Opt. Soc. Am. B* **2009**, *26*, A6.
[48] P. Kadera, J. Sanchez-Pastor, H. Eskandari, T. Tyc, M. Sakaki, M. Schusler, R. Jakoby, N. Benson, A. Jimenez-Saez, J. Lacik, *IEEE Access* **2022**, *10*, 41097.
[49] R. Mendis, D. M. Mittleman, *Opt. Express* **2009**, *17*, 14839.
[50] S.-H. Kim, E. S. Lee, Y. B. Ji, T.-I. Jeon, *Opt. Express* **2010**, *18*, 1289.
[51] H. Guerboukha, R. Shrestha, J. Neronha, Z. Fang, D. M. Mittleman, *Commun. Eng.* **2023**, *2*, 17.
[52] M. Koshiba, *J. Light. Technol.* **2001**, *19*, 1970.
[53] A. Sharkawy, S. Shi, D. W. Prather, *Appl. Opt.* **2001**, *40*, 2247.